MATHEMATICAL MODELING AND COMPUTING, Vol. 7, No. 1, pp. 64–78 (2020)

Modeling Computing Mathematical

Influence of uniaxial and hydrostatic pressures and shear stress σ_5 on the phase transition and thermodynamic properties of quasi-one-dimensional ferroelectrics of the CsH_2PO_4 type

Vdovych A. S.[1], Zachek I. R.[2], Levitskii R. R.[1], Moina A. P.[1]

[1] *Institute for Condensed Matter Physics, 1 Svientsitskii Str., 79011, Lviv, Ukraine*
[2] *Lviv Polytechnic National University, 12 S. Bandera Str., 79013, Lviv, Ukraine*

(Received 10 November 2019; Revised 12 January 2020; Accepted 13 January 2020)

Within the framework of the modified proton ordering model for the quasi-one-dimensional hydrogen bonded ferroelectrics of the CsH_2PO_4 type with taking into account the linear in the strains ε_1, ε_2, ε_3, and ε_5 contributions into the energy of the proton subsystem, without tunneling, using the two-particle cluster approximation, we study the influence of uniaxial pressures p_i, hydrostatic pressure p_h, and shear stress σ_5 on the phase transition, polarization, transverse dielectric permittivity, elastic constants and piezoelectric coefficients of the quasi-one-dimensional CsH_2PO_4 ferroelectric crystals.

Keywords: *ferroelectrics, dielectric permittivity, piezoelectric moduli, shear stress.*

2010 MSC: 82D45, 82B20 **DOI:** 10.23939/mmc2020.01.064

1. Introduction

Investigation of the effects of external pressures and fields is one of the topical problems of the ferroelectrics physics. Using high pressures in experimental studies allows one to obtain additional valuable information about the details of the behavior of the physical characteristics of ferroelectric compounds and to search for new physical effects, not observed at ambient pressure. It also gives a deeper understanding of the phase transition mechanisms in the studied ferroelectric crystals.

The CsH_2PO_4 (CDP) crystals belong to ferroelectric materials with hydrogen bonds.

Exploring the shape of the P-E-hysteresis curves at lowering temperature at different values of hydrostatic pressure, it has been established that at pressure $p = p_k = 0.33\,\text{GPa}$ and temperature $T_{ck} = 151\,\text{K}$ in CsH_2PO_4 [1, 2] the double hysteresis loops appear, that is, the antiferroelectric phase transition takes place. Neutron diffraction experiments revealed doubling of the unit cell along the a-axis in the antiferroelectric phase of CsH_2PO_4 occurs, and the lattice parameters are the following $a = 15.625\,\text{Å}$, $b = 6.254\,\text{Å}$, $c = 4.886\,\text{Å}$, $\beta = 108.08°$. A significant relative displacements of the Cs^{+1} ions and PO_4^{-3} groups in the (a, c) plane are observed, along with rotations of PO_4 tetrahedra by 36.8° in the opposite directions around the b-axis going through the P atom. The protons on the bonds goind along the b-axis are ordered antiparallel in the neighboring chains. The strain and uncompensated dipole moment of the PO_4^{-3} groups agree with such ordering. Hence, in the antiferroelectric phase the sublattice polarizations are directed along the b-axis and totally cancel each other.

The determined in [3] atomic coordinates allowed the authors to identify the structure of the antiferroelectric phase either as the $P2_1$ or $P2_1/a$ group. From the Raman spectra of CsH_2PO_4 obtained at $p = 0.8\,\text{GPa}$ and $T = 83\,\text{K}$ the conclusion was made [4] that the structure of the antiferroelectric phase should be centrosymmetrical, and the $P2_1/a$ group was suggested.

The influence of hydrostatic pressure on the transition temperature in the partially deuterated $Cs(H_{1-x}D_x)_2PO_4$ ferroelectrics was explored in [1, 2, 5–8].

The temperature dependences of spontaneous polarization of the CsH_2PO_4 at different values of hydrostatic pressure were measured in [2], and those of the longitudinal static dielectric permittivity in [2, 5–7].

An attempt of a theoretical description of the transitions between the paraelectric and ferroelectric phases and between the paraelectric and antiferroelectric phases in CsH_2PO_4 and CsD_2PO_4, as well as of the experimental points for $\varepsilon_{22}(0, T, p)$, has been made in [9]. In the used model the crystal is described as pseudospin Ising chains. The interactions within the chains is taken into account exactly, whereas for the dipole-dipole interactions between the chains the mean field approximation is used. The expressions for the reduced spontaneous polarization, equations for the temperatures of the ferroelectric and antiferroelectric transitions, expressions for $\varepsilon_{22}^{-1}(0, T, p)$ were obtained. To describe the experimental $T_c(p)$ dependence it has been assumed that the interaction between the chains changes its sign, when the pressure exceeds the critical one, whereas the intrachain interaction decreases $J_{11} = J_{11}(0) - kp$. No attempt to describe within the proposed theory the experimental data of [1, 2, 8] was made.

The generalized model of the CsH_2PO_4 crystal has been proposed in [10], within which, using the two-particle cluster approximation for the short-range configurational interactions between protons on the shorter hydroge bonds, and with taking into account the long-range interactions between these bonds, the thermodynamic and dynamic characteristics of the CsH_2PO_4 type crystals were calculated. Influence of hydrostatic pressure on the considered compounds is studied, following [11,12], by assuming monotonous dependences of the model parameters on pressure.

In [13, 14] the model of the deformed CsH_2PO_4 crystal is proposed, where the interaction between the pseudospins in the chains is taken into account in the two-particle cluster approximation and between the chains in the mean field approximation. It also takes into account the strains ε_i, ε_5, present in the crystal even at zero pressures [15]. The temperature dependences of the static and dynamic dielectric permittivity of mechanically free crystal and piezoelectric characteristics were calculated for the ferroelectric phase and elastic characteristics for both phases. However, since experimental data for the piezoelectric characteristics are absent, the performed in [14] calculations of these quantities are just some qualitative estimations. Only the calculated in [16] "seed" coefficients of piezoelectric strain $d\ {}^{0}_{2l}$ allow us to obtain adequate with respect to the sign and magnitude results for the piezoelectric characteristics.

In the present paper, using the proposed in [13] model of a deformed crystal of the CsH_2PO_4 type, we study the influence of the uniaxial pressures p_i, hydrostatic pressure p_h, and shear stress σ_5 with the magnitudes up to 0.5 GPa on the phase transition and physical characteristics of the quasi-one-dimensional CDP ferroelectrics and of the hydrostatic pressure p_h as high as 3 GPa on its piezoelectric characteristics.

2. The Hamiltonian of the CsH_2PO_4 crystal

We shall consider the system of protons in the CsH_2PO_4 crystals, moving in the short O-H...O bonds, forming zig-zag chains along the b-axis. As the primitive cell of the Bravais lattice we choose the elementary cell of the antiferroelectric phase ($T < T_N$ and $p > p_k$) Its projection onto the (001) plane is shown in Fig. 1. It corresponds to the antiferroelectric phase ($T < T_N$ and $p > p_k$), and it is larger than the actual cells at $p < p_k$. This cell is formed by two chains, each containing two neighboring PO_4 tetrahedra along with two short hydrogen bonds, belonging to one of them (the "A" type tetrahedron). The hydrogen bonds, attached to the other tetrahedron (of the "B" type), belong to the nearest structure elements, surrounding it.

The Hamiltonian of the proton subsystem of CsH_2PO_4 with taking into account the short-range and long-range interactions consists of the "seed" and pseudospin parts. The "seed" energy U_{seed} describes the heavy ion lattice and does not explicitly depends on the configuration of the proton subsystem. The pseudospin part takes into account the short-range $\hat{H}_{short}$ and long-range $\hat{H}_{MF}$ interactions between

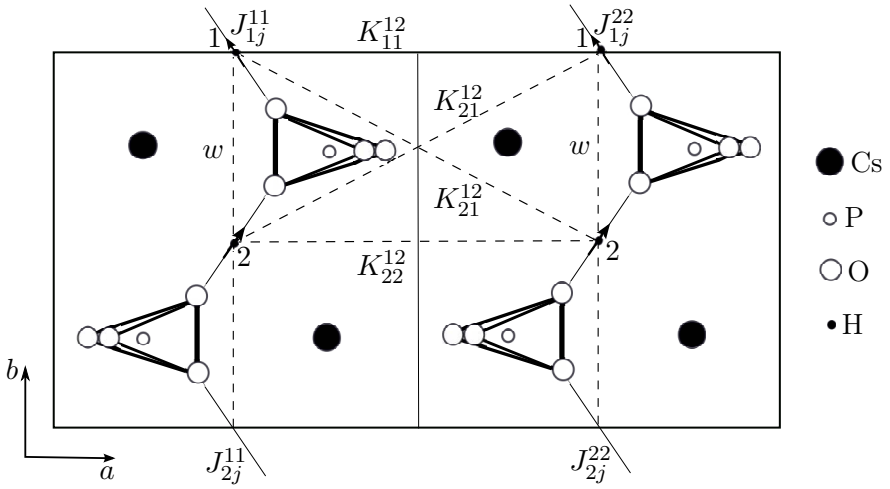

Fig. 1. Primitive cell of the CsH_2PO_4 crystal.

protons that sit near the PO_4 groups, as well as the effective interaction with the electric field E_2. Hence,

$$\hat{H} = NU_{seed} + \hat{H}_{short} + \hat{H}_{long} + \hat{H}_E + \hat{H}'_E, \tag{1}$$

where N is the total number of the primitive cells of the Bravais lattice.

The "seed" energy is expressed via the lattice strains ε_i, $(i = 1, 2, 3)$, ε_5, electric field E_2 and consists of the elastic, piezoelectric, and dielectric parts

$$U_{seed} = v_2 \left\{ \frac{1}{2} \sum_{i,j=1}^{3} c_{ij}^{E0} \varepsilon_i \varepsilon_j + \sum_{i=1}^{3} c_{i5}^{E0} \varepsilon_i \varepsilon_5 - \sum_{i=1}^{3} e_{2i}^0 E_2 \varepsilon_i - e_{25}^0 E_2 \varepsilon_5 - \frac{1}{2} \chi_{22}^{\varepsilon 0} E_2^2 \right\}, \tag{2}$$

where c_{ij}^{E0}, c_{i5}^{E0}, c_{55}^{E0}, e_{2i}^0, e_{25}^0, $\chi_{22}^{\varepsilon 0}$ are the "seed" elastic constants, the piezoelectric voltage coefficients, and the dielectric susceptibility of mechanically clamped crystal.

The Hamiltonian of the short-range interactions is

$$\hat{H}_{short} = -2w \sum_{qq'} \left(\frac{\sigma_{q1}^A}{2} \frac{\sigma_{q2}^A}{2} + \frac{\sigma_{q1}^B}{2} \frac{\sigma_{q2}^B}{2} \right) \left(\delta_{\mathbf{R}_q \mathbf{R}_{q'}} + \delta_{\mathbf{R}_q + \mathbf{r}, \mathbf{R}_{q'}} \right). \tag{3}$$

The first and second Kronecker symbols corresponds to the proton interactions in the chains near the "A" and "B" type tetrahedra, respectively; $\mathbf{r}$ is the position vector of the proton bond within the cell. The parameter w, describing the short-range interactions between protons within the same chain, is expanded in the strains ε_i, ε_5 up to the linear terms

$$w = w^0 + \sum_l \delta_{2l} \varepsilon_l, \quad (l = 1, 2, 3, 5). \tag{4}$$

$\hat{H}_{long}$ is the mean field Hamiltonian of the long-range dipole-dipole and indirect lattice mediated interactions between protons

$$\begin{aligned} \hat{H}_{long} = {} & \frac{1}{2} \sum_{\substack{qq' \\ ff'}} \sum_{l=1}^{2} J_{ff'}^{ll}(qq') \frac{\langle \sigma_{qf}^{(l)} \rangle}{2} \frac{\langle \sigma_{q'f'}^{(l)} \rangle}{2} - \sum_{\substack{qq' \\ ff'}} \sum_{l=1}^{2} J_{ff'}^{ll}(qq') \frac{\langle \sigma_{q'f'}^{(l)} \rangle}{2} \frac{\sigma_{qf}^{(l)}}{2} \\ & - \frac{1}{2} \sum_{\substack{qq' \\ ff'}} \sum_{ll'} K_{ff'}^{ll'}(qq') \frac{\langle \sigma_{qf}^{(l)} \rangle}{2} \frac{\langle \sigma_{q'f'}^{(l')} \rangle}{2} - \sum_{\substack{qq' \\ ff'}} \sum_{ll'} K_{ff'}^{ll'}(qq') \frac{\langle \sigma_{q'f'}^{(l')} \rangle}{2} \frac{\sigma_{qf}^{(l)}}{2}. \end{aligned} \tag{5}$$

Here the two first terms describe the effective long-range interactions between protons of the same sublattice "A" or "B", whereas the two subsequent terms correspond to interactions between protons of different sublattices "A" and "B". Expanding the constants of the long-range interactions in the strains ε_i, ε_j and retaining only linear terms,

$$J_{11} = J_{22} = J_1 + \sum_l \bar{\varphi}_{1l}\varepsilon_l, \qquad J_{12} = J_{21} = J_2 + \sum_l \bar{\varphi}_{2l}\varepsilon_l, \tag{6}$$
$$K_{11} = K_{22} = K_1 + \sum_l \varphi_{1l}\varepsilon_l, \qquad K_{12} = K_{21} = K_2 + \sum_l \varphi_{2l}\varepsilon_l,$$

where $J_{ff'} = \sum_{\mathbf{R}_q - \mathbf{R}_{q'}} J_{ff'}(qq')$, $K_{ff'} = \sum_{\mathbf{R}_q - \mathbf{R}_{q'}} K_{ff'}(qq')$ are the Fourier transforms of the long-range interaction constants, taking into account the symmetry of the single-particle distribution functions at ferroelectric ordering

$$\langle \sigma_{q1}^A \rangle = \langle \sigma_{q2}^A \rangle = \eta_1, \qquad \langle \sigma_{q1}^B \rangle = \langle \sigma_{q2}^B \rangle = \eta_2 \tag{7}$$

we obtain

$$\hat{H}_{long} = NH^0 + \hat{H}_2, \tag{8}$$

whereas the expressions for H^0, H_2 read

$$\hat{H}^0 = \nu_1(\eta_1^2 + \eta_2^2) + 2\nu_2\eta_1\eta_2, \tag{9}$$

$$\hat{H}_2 = \sum_q \left\{ -(2\nu_1\eta_1 + 2\nu_2\eta_2)\left(\frac{\sigma_{q1}^A}{2} + \frac{\sigma_{q2}^A}{2}\right) - (2\nu_2\eta_1 + 2\nu_1\eta_2)\left(\frac{\sigma_{q1}^B}{2} + \frac{\sigma_{q2}^B}{2}\right)\right\}. \tag{10}$$

Here the following notations are used

$$\nu_1 = \frac{1}{8}(J_{11} + J_{22} + 2J_{12}) = \nu_1^0 + \sum_l \psi_{l1}\varepsilon_l, \qquad \nu_1^0 = \frac{1}{4}(J_1 + J_2), \qquad \psi_{l1} = \frac{1}{4}(\bar{\varphi}_{1l} + \varphi_{1l}), \tag{11}$$

$$\nu_2 = \frac{1}{8}(K_{11} + K_{22} + 2K_{12}) = \nu_2^0 + \sum_l \psi_{l2}\varepsilon_l, \qquad \nu_2^0 = \frac{1}{4}(K_1 + K_2), \qquad \psi_{l2} = \frac{1}{4}(\bar{\varphi}_{2l} + \varphi_{2l}). \tag{12}$$

The fourth term in (1) describes the interaction of pseudospins with the electric field

$$\hat{H}_E = -\sum_q \mu_y E_2 \left(\frac{\sigma_{q1}^A}{2} + \frac{\sigma_{q2}^A}{2} + \frac{\sigma_{q1}^B}{2} + \frac{\sigma_{q2}^B}{2}\right), \tag{13}$$

where μ_y is the projection of the effective dipole moment of a pseudospin on the axis y.

The therm $\hat{H}'_E$ in the Hamiltonian (1) describes the mentioned above dependence of the longitudinal components of the dipole moments on the pseudospin mean values

$$\hat{H}'_E = -\sum_{qf} s_f^2 \mu' E_2 \frac{\sigma_{qf}}{2} = -\sum_{qf} \left(\frac{1}{N}\sum_{q'} \sigma_{q'f}\right)^2 \mu' E_2 \frac{\sigma_{qf}}{2}. \tag{14}$$

where N is the number of unit cells; σ_{qf} is the shortened notation of the σ_{q1}^A, σ_{q2}^A, σ_{q1}^B, σ_{q2}^B pseudospins. The corrections to the dipole moments have the form $s_f^2\mu'$, and not $s_f\mu'$, because of the symmetry considerations: the system energy should not change at reversing the signs of the field and all pseudospins.

The term $\hat{H}'_E$, just like the long-range interactions, is taken into account in the mean field approximation

$$\hat{H}'_E = -\sum_{qf} \left(\frac{1}{N}\sum_{q'} \sigma_{q'f}\right)^2 \mu' E_2 \frac{\sigma_{qf}}{2}$$

$$= -\frac{1}{N^2}\sum_{qf}\sum_{q'}\sum_{q''}\sigma_{qf}\sigma_{q'f}\sigma_{q''f}\frac{\mu' E_2}{2}$$
$$\approx -\frac{1}{N^2}\sum_{qf}\sum_{q'}\sum_{q''}\left((\sigma_{qf}+\sigma_{q'f}+\sigma_{q''f})\eta_f^2 - 2\eta_f^3\right)\frac{\mu' E_2}{2}$$
$$= -3\sum_{q}\sum_{f=1}^{4}\frac{\sigma_{qf}}{2}\eta_f^2\mu' E_2 + N\sum_{f=1}^{4}\eta_f^3\mu' E_2. \tag{15}$$

When Eq. (7) is taken into account, the expression (15) is simplified

$$\hat{H}'_E = -3\sum_{q}\mu' E_2\left(\frac{\eta_1^2\sigma_{q1}^A}{2}+\frac{\eta_1^2\sigma_{q2}^A}{2}+\frac{\eta_2^2\sigma_{q1}^B}{2}+\frac{\eta_2^2\sigma_{q2}^B}{2}\right)+2N\left(\eta_1^3+\eta_2^3\right)\mu' E_2. \tag{16}$$

The thermodynamic characteristics of CDP are calculated using the two-particle cluster approximation (TPCA).

3. Static longitudinal dielectric, piezoelectric, elastic and thermal characteristics of CsH_2PO_4

The thermodynamic potential of the proton subsystem of CDP per one primitive cell can be written as

$$g = v_2 U_{seed} + H^0 + 2\left(\eta_1^3+\eta_2^3\right)\mu' E_2 + 2k_BT\ln 2 - 2w - v_2\sum_l \sigma_l\varepsilon_l$$
$$- k_BT\ln(1-\eta_1^2) - k_BT\ln(1-\eta_2^2) - 2k_BT\ln D, \tag{17}$$

where

$$\eta_1 = \frac{1}{D}\left[\sinh(y_1+y_2)+\sinh(y_1-y_2)+2a\sinh y_1\right],$$
$$\eta_2 = \frac{1}{D}\left[\sinh(y_1+y_2)-\sinh(y_1-y_2)+2a\sinh y_2\right]. \tag{18}$$

Here the following notations are used

$$D = \cosh(y_1+y_2)+\cosh(y_1-y_2)+2a\cosh y_1+2a\cosh y_2+2a^2,$$
$$a = e^{-\frac{w}{k_BT}},$$
$$y_1 = \frac{1}{2}\ln\frac{1+\eta_1}{1-\eta_1}+\beta\nu_1\eta_1+\beta\nu_2\eta_2+\frac{1}{2}\beta\left(\mu_y E_2+3\eta_1^2\mu' E_2\right),$$
$$y_2 = \frac{1}{2}\ln\frac{1+\eta_2}{1-\eta_2}+\beta\nu_2\eta_1+\beta\nu_1\eta_2+\frac{1}{2}\beta\left(\mu_y E_2+3\eta_2^2\mu' E_2\right).$$

Using the equilibrium conditions, we obtain the system of equations for the strains ε_j

$$\sigma_l = c_{l1}^{E0}\varepsilon_1 + c_{l2}^{E0}\varepsilon_2 + c_{l3}^{E0}\varepsilon_3 + c_{l5}^{E0}\varepsilon_5 - e_{21}^0 E_2 - \frac{2\delta_l}{v_2}+\frac{4\delta_l}{v_2 D}M$$
$$-\frac{1}{v_2}\psi_{l1}\left(\eta_1^2+\eta_2^2\right)-\frac{2}{v_2}\psi_{l2}\eta_1\eta_2, \tag{19}$$

where

$$M = \left[a\cosh y_1 + a\cosh y_2 + 2a^2\right].$$

From the thermodynamic potential (17) expressions for different thermodynamic characteristics can be easily obtained. Thus the longitudinal polarization P_2 reads

$$P_2 = -\left(\frac{\partial g}{\partial E_2}\right)_{\sigma_i} = \sum_j e^0_{2j}\varepsilon_j + \chi^{\varepsilon 0}_{22}E_2 + \frac{\mu_y}{v_2}(\eta_1+\eta_2) + \frac{\mu'}{v_2}(\eta_1^3+\eta_2^3). \tag{20}$$

The isothermal static susceptibility of mechanically clamped crystal is

$$\begin{aligned}\chi^{\varepsilon T}_{22} = \left(\frac{\partial P_2}{\partial E_2}\right)_{\varepsilon_i} &= \chi^{\varepsilon 0}_{22} + \frac{\beta\tilde{\mu}^2_{1y}}{2v_2\Delta}\left\{D(\varkappa_{11}+\varkappa_{12}) - (\tilde{\varphi}_2-\beta\nu_2)(\varkappa_{11}\varkappa_{22}-\varkappa^2_{12})\right\}\\ &+ \frac{\beta\tilde{\mu}^2_{2y}}{2v_2\Delta}\left\{D(\varkappa_{12}+\varkappa_{22}) - (\tilde{\varphi}_1-\beta\nu_2)(\varkappa_{11}\varkappa_{22}-\varkappa^2_{12})\right\},\end{aligned} \tag{21}$$

where the following notations are used

$$\begin{aligned}\Delta &= D^2 - D\left[\tilde{\varphi}_1\varkappa_{11}+\tilde{\varphi}_2\varkappa_{22}+2\beta\nu_2\varkappa_{12}\right] + \left[\tilde{\varphi}_1\tilde{\varphi}_2-(\beta\nu_2)^2\right](\varkappa_{11}\varkappa_{22}-\varkappa^2_{12}),\\ \tilde{\varphi}_1 &= \varphi_1 + 3\eta_1\beta\mu' E_2, \quad \tilde{\varphi}_2 = \varphi_2 + 3\eta_2\beta\mu' E_2, \quad \varphi_1 = \frac{1}{1-\eta_1^2}+\beta\nu_1, \quad \varphi_2 = \frac{1}{1-\eta_2^2}+\beta\nu_1,\\ \tilde{\mu}_{1y} &= \mu_y + 3\mu'\eta_1^2, \quad \tilde{\mu}_{2y} = \mu_y + 3\mu'\eta_2^2,\\ \varkappa_{11} &= \cosh(y_1+y_2)+\cosh(y_1-y_2)+2a\cosh y_1 - \eta_1^2 D,\\ \varkappa_{12} &= \cosh(y_1+y_2)-\cosh(y_1-y_2)-\eta_1\eta_2 D,\\ \varkappa_{22} &= \cosh(y_1+y_2)+\cosh(y_1-y_2)+2a\cosh y_2 - \eta_2^2 D.\end{aligned}$$

The isothermal piezoelectric voltage coefficients are

$$e^T_{2l} = \left(\frac{\partial P_2}{\partial\varepsilon_l}\right)_{E_2} = e^0_{2l} + \frac{1}{v_2}\left(\tilde{\mu}_{1y}\eta_1^{\prime(l)} + \tilde{\mu}_{2y}\eta_2^{\prime(l)}\right), \quad (l=1,2,3,5),$$

where

$$\begin{aligned}\eta_1^{\prime(l)} &= \frac{\beta}{\Delta}\big\{(\psi_{l1}\eta_1+\psi_{l2}\eta_2)[D(\varkappa_{11}+\varkappa_{12}) - (\tilde{\varphi}_2-\beta\nu_2)(\varkappa_{11}\varkappa_{22}-\varkappa^2_{12})]\\ &\quad - \delta_l[D\rho_1 - \rho_1(\beta\nu_2\varkappa_{12}+\tilde{\varphi}_2\varkappa_{22}) + \rho_2(\beta\nu_2\varkappa_{11}+\tilde{\varphi}_2\varkappa_{12})]\big\},\\ \eta_2^{\prime(l)} &= \frac{\beta}{\Delta}\big\{(\psi_{l2}\eta_1+\psi_{l1}\eta_2)[D(\varkappa_{22}+\varkappa_{12}) - (\tilde{\varphi}_1-\beta\nu_2)(\varkappa_{11}\varkappa_{22}-\varkappa^2_{12})]\\ &\quad - \delta_l[D\rho_2 + \rho_1(\beta\nu_2\varkappa_{22}+\tilde{\varphi}_1\varkappa_{12}) - \rho_2(\beta\nu_2\varkappa_{12}+\tilde{\varphi}_1\varkappa_{11})]\big\},\\ \rho_1 &= 2a\sinh y_1 - \eta_1[2a\cosh y_1 + 2a\cosh y_2 + 4a^2],\\ \rho_2 &= 2a\sinh y_2 - \eta_2[2a\cosh y_1 + 2a\cosh y_2 + 4a^2].\end{aligned}$$

The piezoelectric stress constants are obtained by differentiation of electric field over strains at constant polarization:

$$h_{2i} = -\left(\frac{\partial E_2}{\partial\varepsilon_i}\right)_{P_2} = \frac{e_{2i}}{\chi^{\varepsilon}_{22}}. \tag{22}$$

The calculations of the isothermal elastic constants at constant field yield

$$\begin{aligned}c^E_{il} = \left(\frac{\partial\sigma_i}{\partial\varepsilon_i}\right)_{E_2} &= c^{E0}_{ij} - \frac{2}{v_2}\left(\psi_{i1}\eta_1+\psi_{i2}\eta_2+\frac{\delta_i}{D}\varkappa^c_1\varphi_1+\frac{\delta_i}{D}\varkappa^c_2\beta\nu_2\right)\eta_1^{\prime(l)}\\ &\quad - \frac{2}{v_2}\left(\psi_{i1}\eta_2+\psi_{i2}\eta_1+\frac{\delta_i}{D}\varkappa^c_1\beta\nu_2+\frac{\delta_i}{D}\varkappa^c_2\varphi_2\right)\eta_2^{\prime(l)}\\ &\quad - \frac{2\beta\delta_i}{v_2 D}\left[\psi_{l1}(\varkappa^c_1\eta_1+\varkappa^c_2\eta_2)+\psi_{l2}(\varkappa^c_2\eta_1+\varkappa^c_1\eta_1)\right] - \frac{4\beta\delta_i\delta_l}{D}\rho^c,\end{aligned} \tag{23}$$

where

$$\varkappa_1^c = \sinh(y_1+y_2)+\sinh(y_1-y_2)-\eta_1[\cosh(y_1+y_2)+\cosh(y_1-y_2)-2a^2],$$
$$\varkappa_2^c = \sinh(y_1+y_2)-\sinh(y_1-y_2)-\eta_2[\cosh(y_1+y_2)+\cosh(y_1-y_2)-2a^2],$$
$$\rho^c = 2a^2+\frac{\left[\cosh(y_1+y_2)+\cosh(y_1-y_2)-2a^2\right]}{D}\left[a\cosh y_1+a\cosh y_2+2a^2\right].$$

Other dielectric, piezoelectric, and elastic characteristics of CsH_2PO_4 can be obtained from the found above characteristics. Thus, the isothermal piezoelectric strain constants are

$$d_{2i}^T = \sum_j s_{ij}^E e_{2j}^T, \quad (i,j=1,2,3,5). \tag{24}$$

The matrix of the isothermal susceptibilities at constant field s_{ij}^E is inverse to the matrix of elastic constants c_{ij}^E:

$$\widehat{C^E} = \begin{pmatrix} c_{11}^E & c_{12}^E & c_{13}^E & c_{15}^E \\ c_{12}^E & c_{22}^E & c_{23}^E & c_{25}^E \\ c_{13}^E & c_{23}^E & c_{33}^E & c_{35}^E \\ c_{15}^E & c_{25}^E & c_{35}^E & c_{55}^E \end{pmatrix}, \qquad \widehat{S^E} = (\widehat{C^E})^{-1}.$$

The isothermal piezoelectric strain coefficients are

$$g_{2i}^T = \sum_j s_{ij}^P h_{2j}^T. \tag{25}$$

4. Comparison of numerical calculations with the experimental data. Discussion of the obtained results

It should be noted that the developed in the previous sections theory, strictly speaking, is valid for the deuterated quasi-one-dimensional ferroelectrics only. However, the thermodynamic and dynamic properties of hydrogen bonded ferroelectrics with tunneling Ω are determined by the effective tunneling parameter $\bar{\Omega}$, renormalized by the short-range interactions [17]. Since $\bar{\Omega} \ll \Omega$, the essential suppression of tunneling by the short-range interactions takes place. We shall assume that the presented in the previous sections results are valid for CDP crystals as well.

In order to calculate within the proposed theory the temperature dependences of the corresponding physical characteristics of the CDP crystal at different pressures, we need to set the values of the following parameters:

the two-particle cluster parameter w;
long-range interaction parameters ν_s;
effective dipole moments μ_2;
deformation potentials δ_i, δ_5, ψ_{is}, ψ_{5s};
"seed" dielectric susceptibilities $\chi_{22}^{\varepsilon 0}$;
"seed" coefficients of piezoelectric напруги e_{2i}^0, e_{25}^0;
"seed" elastic constants c_{ij}^{E0}, c_{i5}^{E0}, c_{55}^{E0}.

In the fitting procedure we use the experimental data for the physical characteristics of CDP, namely, for $P_s(T)$ [15], $\varepsilon_i(T)$, $\varepsilon_5(T)$ [15].

The "seed" piezoelectric voltage coefficients e_{2i}^0, e_{25}^0 are determined from the expressions $e_{2l}^0 = \sum_{i=1}^l C_{il}^E d_{\ 2l}^{\ 0}$, where the values of $d_{\ 2l}^{\ 0}$ are taken from [16], which are calculated relative to the axis OX ($d_{21}^0 = 14.59\cdot 10^{-8}$ esu/dyn, $d_{22}^0 = -6.33\cdot 10^{-8}$ esu/dyn, $d_{23}^0 = -1.39\cdot 10^{-8}$ esu/dyn^2, $d_{25}^0 = -11.93\cdot 10^4$ esu/dyn^2). As a result, we obtain $e_{21}^0 = 2.2767\cdot 10^4$ esu/cm^2, $e_{22}^0 = -1.2286\cdot 10^4$ esu/dyn, $e_{23}^0 = 3.6323\cdot 10^4$ esu/dyn, $e_{25}^0 = -0.5079\cdot 10^4$ esu/cm^2. The elastic constants C_{il} are calculated, using Eq. (23). The physical characteristics are calculated in the vicinity of the transition temperature with an accuracy of 0.002 K.

The primitive cell volume of CDP is taken to be $v_2 = 0.467 \cdot 10^{-21}$ cm^3.

The value of the effective dipole moment is assumed to be dependent on hydrostatic pressure p as $\mu_y = \mu_y^0 + k_p p$. In the present work we take $k_p = 0.2 \cdot 10^{-18} \frac{\text{esu}\cdot\text{cm}^3}{\text{dyn}}$

The obtained optimal set of the model parameters is given in Tables 1.

Table 1. The set of the theory parameters for the CDP crystal.

T_c, K	$\frac{w}{k_B}$	$\frac{\nu_1}{k_B}$, K	$\frac{\nu_2}{k_B}$, K	μ_y, 10^{-18}, K	μ', 10^{-18}, esu · cm	$\chi_{22}^{\varepsilon 0}$, esu · cm
153	640.3	1.75	0.45	2.7	0.5	0.443

$\frac{\delta_1}{k_B}$	$\frac{\delta_2}{k_B}$, K	$\frac{\delta_3}{k_B}$, K	$\frac{\delta_5}{k_B}$, K	$\frac{\psi_{11}}{k_B}$, K	$\frac{\psi_{21}}{k_B}$, K	$\frac{\psi_{31}}{k_B}$, K	$\frac{\psi_{51}}{k_B}$, K
187.6	−67.7	288.2	−22.2	175.8	−63.5	270.2	−20.8

The "seed" parameters c_{il}^{0E} are [18]: $c_{11}^{0E} = 28.83 \cdot 10^{10}$ $\frac{\text{dyn}}{\text{cm}^2}$, $c_{12}^{E0} = 11.4 \cdot 10^{10}$ $\frac{\text{dyn}}{\text{cm}^2}$, $c_{13}^{E0} = 42.87 \cdot 10^{10}$ $\frac{\text{dyn}}{\text{cm}^2}$, $c_{22}^{E0} = 26.67 \cdot 10^{10}$ $\frac{\text{dyn}}{\text{cm}^2}$, $c_{23}^{E0} = 14.5 \cdot 10^{10}$ $\frac{\text{dyn}}{\text{cm}^2}$, $c_{33}^{E0} = 65.45 \cdot 10^{10}$ $\frac{\text{dyn}}{\text{cm}^2}$, $c_{15}^{E0} = 5.13 \cdot 10^{10}$ $\frac{\text{dyn}}{\text{cm}^2}$, $c_{25}^{E0} = 8.4 \cdot 10^{10}$ $\frac{\text{dyn}}{\text{cm}^2}$, $c_{35}^{E0} = 7.50 \cdot 10^{10}$ $\frac{\text{dyn}}{\text{cm}^2}$, $c_{55}^{E0} = 5.20 \cdot 10^{10}$ $\frac{\text{dyn}}{\text{cm}^2}$.

Let us discuss the obtained results. We shall analyze the influence of hydrostatic $p_h = -\sigma_1 = -\sigma_2 = -\sigma_3$ and uniaxial $p_i = -\sigma_i$ pressures and shear stress $p = -\sigma_5$ on the thermodynamic characteristics of the CDP crystal.

Let us note, that we are not aware of any experimental studies of the uniaxial pressures $p_i = -\sigma_i$ or shear stress $p = \sigma_5$ effects on the thermodynamic characteristics of these crystals. The obtained here results, therefore, estimate the effects of these stresses only qualitatively. Experimental measurements will allow us to determine the values of the model parameters more precisely and describe the new experimental data quantitatively.

Fig. 2 illustrates the dependence of the transition temperature T_c on hydrostatic and uniaxial pressures and the shear strain σ_5.

Pressures p_1, p_h and stress σ_5 decreases the transition temperature T_c, whereas the uniaxial pressures p_2, p_3 increase it. The rate of the pressure changes $\frac{dT_c}{dp_1}$ is the largest.

The calculated with the accepted values of the model parameters dependences $T_c(p)$ quantitatively well describe the experimental data of [1] both at $p < p_k$ and $p > p_k$, as well as the data of [5]. The transition temperature in the CDP crystals decreases with the rate $\frac{dT_c}{dp} = -56\,\text{K/GPa}$ [8]; $-85\,\text{K/GPa}$ [1]; $-110\,\text{K/GPa}$ [5]; $-68\,\text{K/GPa}$ [7].

The temperature dependences of the strains ε_l of the CDP crystal at ambient pressure are presented in Fig. 3a, whereas the influence of the pressure p_h, shear stress σ_5, and uniaxial pressures p_1, p_2, p_3 on these dependences is illustrated in Figs. 3b–3f.

The calculations show that the temperature and pressure curves of the strains ε_i and ε_5 are determined, mainly, by the values of the "seed" elastic constants c_{ij}^{E0} [18], whereas the effects of the deformation potentials δ_i, δ_5, φ_i, φ_5 on the strains ε_i and ε_5 are very insignificant.

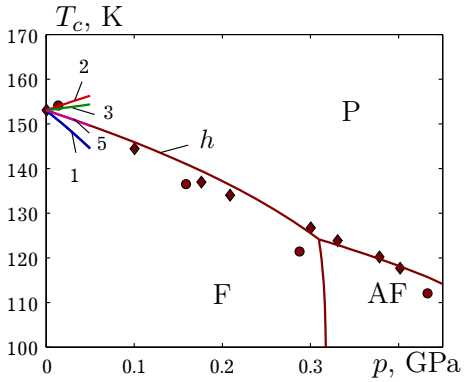

Fig. 2. Dependence of the temperature T_c of the transition between the paraelectric and ferroelectric phase of CDP on the uniaxial pressures p_1 — 1, p_2 — 2, p_3 — 3, hydrostatic pressure p — h, ♦ — [1], • — [5] and shear stress σ_5 — 5.

The pressure-induced changes in the strains ε_l change the values of the theory parameters w, ν_1, ν_2, shifting thereby the transition temperature. With increasing p_1, p_h, and σ_5 the parameter of the short-range interactions w decreases, with $w_1 < w_5 < w_h$ and, correspondingly $T_{c1} < T_{c5} < T_{ch}$, whereas with increasing p_2 and p_3 the parameter w increases, with $w_2 > w_3$ and $T_{c2} > T_{c3}$.

The effects of the pressures of different symmetries on the temperature dependences of spontaneous polarization P_s and longitudinal static dielectric permittivity $\varepsilon_{22}(T, p)$ are illustrated in Figs. 4 and 6, respectively.

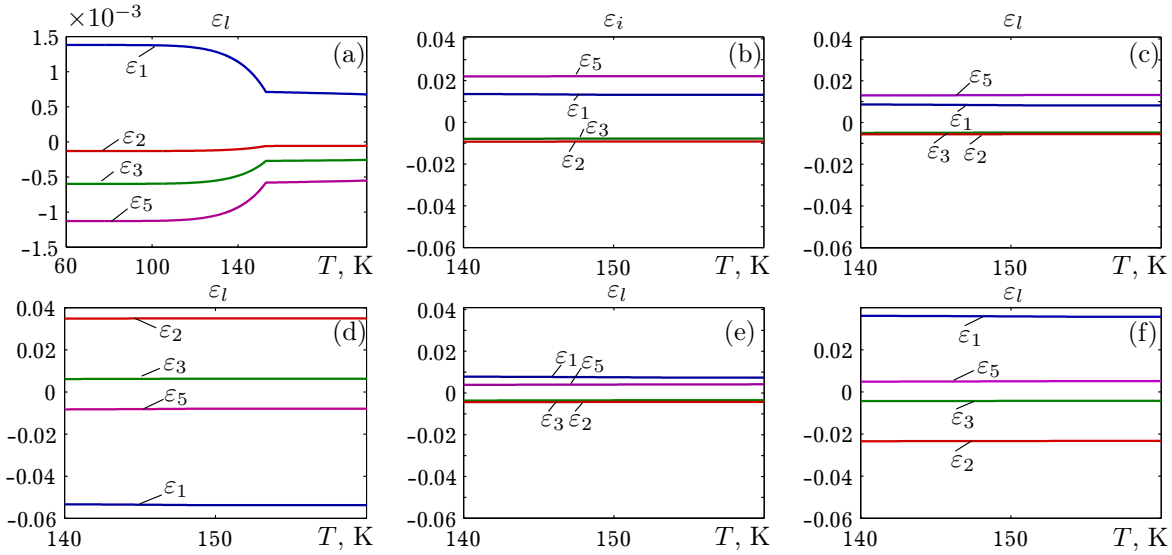

Fig. 3. The temperature dependences of the strains ε_l of the CDP crystals in absence of external pressures (a); under hydrostatic pressure p_h (b); under shear stress σ_5 (c); under uniaxial pressures p_1 (d); p_2 (e); p_3 (f) with the magnitude of 0.3 GPa each.

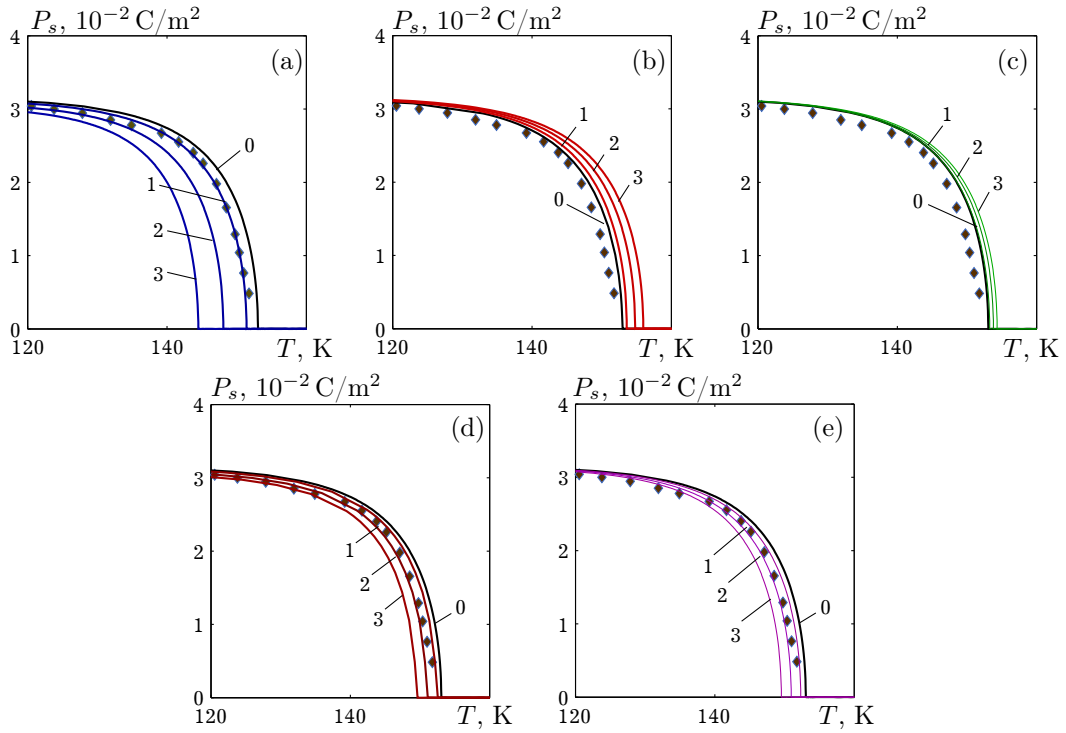

Fig. 4. The temperature dependence of spontaneous polarization of CDP under uniaxial pressures p_1 (a), p_2 (b), p_3 (c), hydrostatic pressure (d), shear stress σ_5 (e) of the following magnitudes (GPa): 0.0 — 0, ♦ [1], 0.1 — 1, 0.3 — 2, 0.5 — 3.

In these figures we plot the temperature dependences of spontaneous polarization P_s, static dielectric permittivity $\varepsilon_{22}(T,p)$ at ambient pressure and under applied uniaxial pressures, hydrostatic pressure, and shear stress σ_5, each with a magnitude of 0.5 GPa. The applied pressures p_1, p_h, the stress σ_5 and the pressures p_2 and p_3 shift the curves of P_s, $\varepsilon_{22}(T,p)$ to lower and to higher temperatures, respectively.

In order to compare the effects of pressures p_i, p_h, and stress σ_5 on P_s, $\varepsilon_{22}(T,p)$, we calculate these characteristics of CDP as functions of the temperature difference $\Delta T = T - T_c$ (see Figs. 5, 7).

Increasing pressures p_1, p_h and stress σ_5 decreases the magnitude of saturation polarization P_s, with $P_{s1} < P_{sh} < P_{s5}$, but increases the dielectric permittivity $\varepsilon_{22}(T,p)$ and $\varepsilon_{22}(5) > \varepsilon_{22}(1) > \varepsilon_{22}(h)$.

On the other hand, pressures p_2 and p_3 increase the polarization P_{s3} and P_{s2} with $P_{s3} < P_{s2}$, but decrease the permittivity $\varepsilon_{22}(2)$ and $\varepsilon_{22}(3)$.

The temperature dependences of the elastic constants c_{il}^E, piezoelectric e_{2l} and strain d_{2l} coefficients, piezoelectric voltage h_{2l} and strain g_{2l} constants at ambient pressure and under applied uniaxial pressures, hydrostatic pressure, and shear stress σ_5, each with a magnitude of 0.5 GPa, are shown in Figs. 8, 9, 10. Also the figures contain the curves calculated at the values of hydrostatic pressure of 2 GPa, 3 GPa as well at 3.1 GPa, the pressure above the critical one.

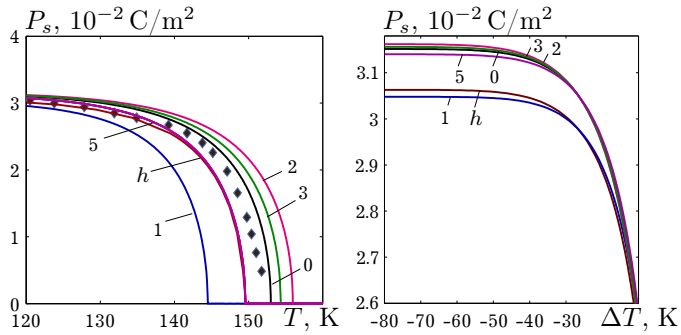

Fig. 5. Dependences of spontaneous polarization of CDP on on temperature T and on the temperature difference $\Delta T = T - T_c$: at ambient pressure — 0, ♦ [1]; at pressures of different symmetries, each with the magnitude of 0.5 GPa: uniaxial p_1 — 1, p_2 — 2, p_3 — 3, hydrostatic — h, shear stress σ_5 — 5.

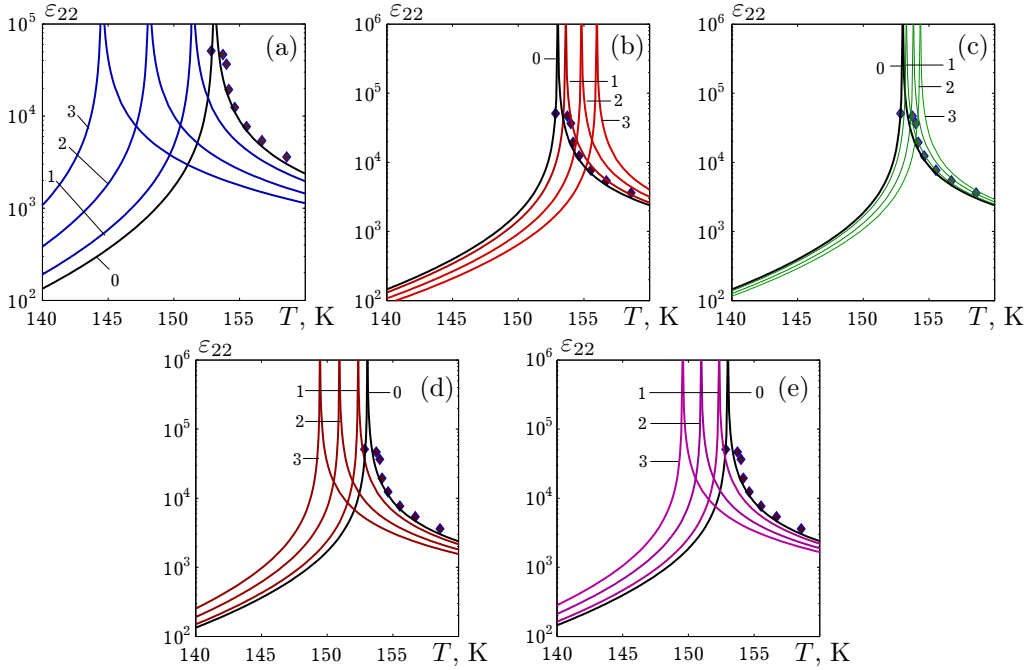

Fig. 6. The temperature dependence of the dielectric permittivity ε_{22} of CDP under uniaxial pressures p_1 — (a), p_2 — (b), p_3 — (c), hydrostatic pressure — (d), shear stress σ_5 — (e) of the following magnitudes (GPa): 0.0 — 0, ♦ [1], 0.1 — 1, 0.3 — 2, 0.5 — 3.

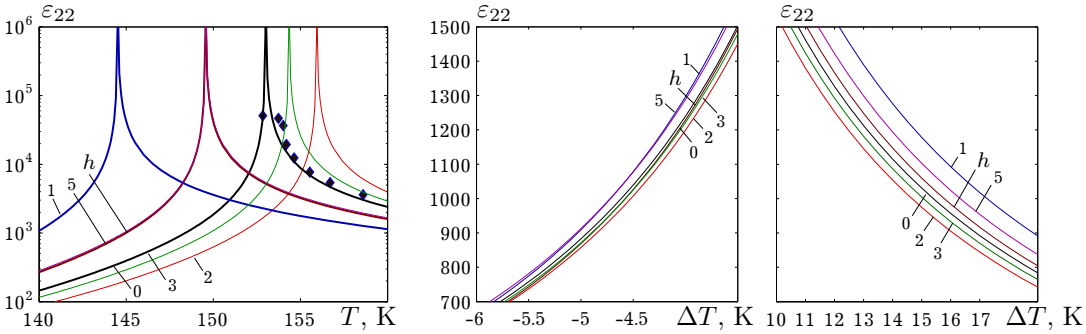

Fig. 7. Dependences of the dielectric permittivity ε_{22} on temperature T and on the temperature difference $\Delta T = T - T_c$: at abmient pressure – 0, ♦ [1]; at pressures of different symmetries, each with the magnitude of 0.5 GPa: uniaxial p_1 — 1, p_2 — 2, p_3 — 3, hydrostatic — h, shear stress σ_5 — 5.

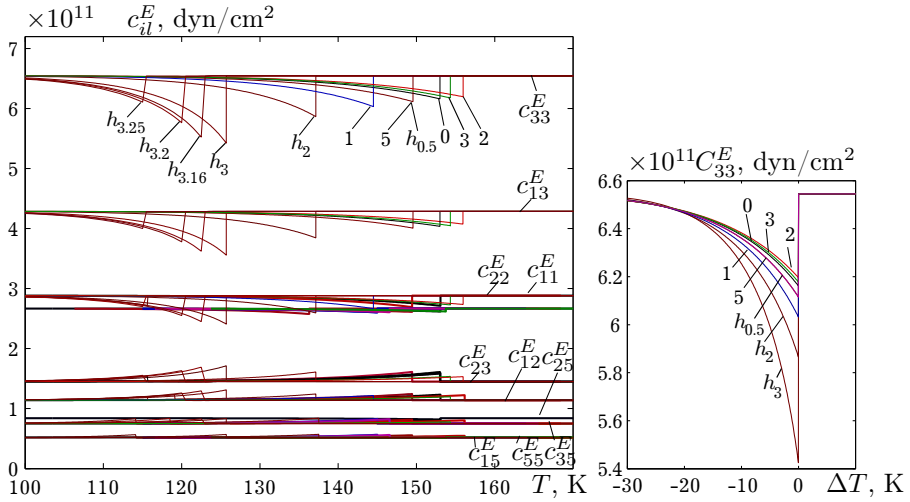

Fig. 8. The temperature dependence of the elastic constants c_{il}^E and the dependence of the elastic constant c_{33}^E on the temperature difference $\Delta T = T - T_c$: at ambient pressure — 0, at pressures of different symmetries, each with the magnitude of 0.5 GPa: uniaxial p_1 — 1, p_2 — 2, p_3 — 3, shear stress σ_5 — 5, and under hydrostatic pressure (GPa): 0.5 — $h_{0.5}$, 2 — h_2, 3 — h_3, 3.12 — $h_{3.12}$, 3.15 — $h_{3.15}$.

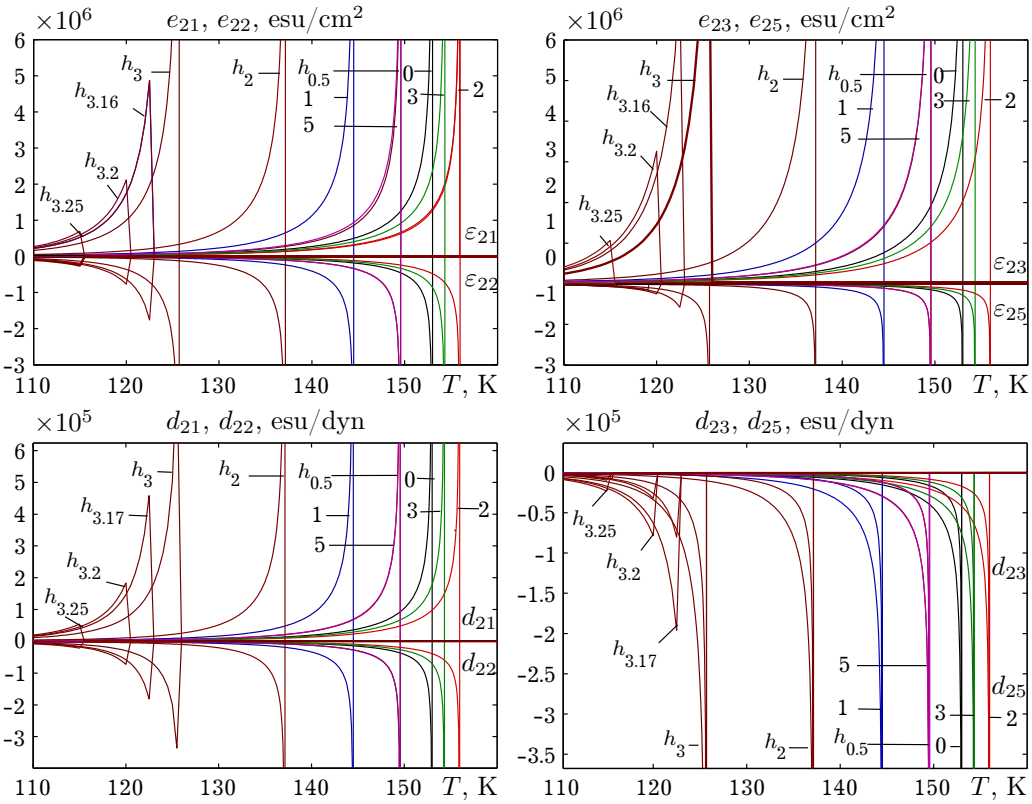

Fig. 9. The temperature dependences of the piezoelectric voltage e_{2l} and strain d_{2l} coefficients: at ambient pressure – 0, at pressures of different symmetries, each with the magnitude of 0.5 GPa: uniaxial p_1 — 1, p_2 — 2, p_3 — 3, shear stress σ_5 — 5, and under hydrostatic pressure (GPa): 0.5 — $h_{0.5}$, 2 — h_2, 3 — h_3, 3.12 — $h_{3.12}$, 3.15 — $h_{3.15}$.

The applied pressures p_1, p_h and the stress σ_5 shift the temperature curves of c_{il}^E, e_{2l}, d_{2l}, h_{2l}, and g_{2l} to lower temperatures, whereas the pressures p_2 and p_3 shift the curves to higher temperatures. The elastic constants c_{11}^E, c_{22}^E, c_{33}^E, C_{13}^E have minima at $T = T_c$, whereas c_{23}^E, c_{12}^E, c_{15}^E, c_{25}^E have maxima.

At hydrostatic pressure above the critical one $p_h > p_{hcr}$ the jumps of the elastic constants c_{il}^E and the maximal values of the piezomoduli e_{2l}, d_{2l} decrease; at pressures $p_h > 3.4$ GPa the jumps of c_{il}^E

vanish, whereas the piezomoduli e_{2l}, d_{2l} coincide with their "seed" values. At pressures above p_{hcr} the temperature curves of the piezoelectric voltage and strain constants have downward jumps at $T = T_N$.

With increasing pressures p_2 and p_3 the jumps of the elastic constant c_{33}^E increase, whereas the pressures p_1, p_h, and stress σ_5 decrease c_{33}^E (Fig. 8).

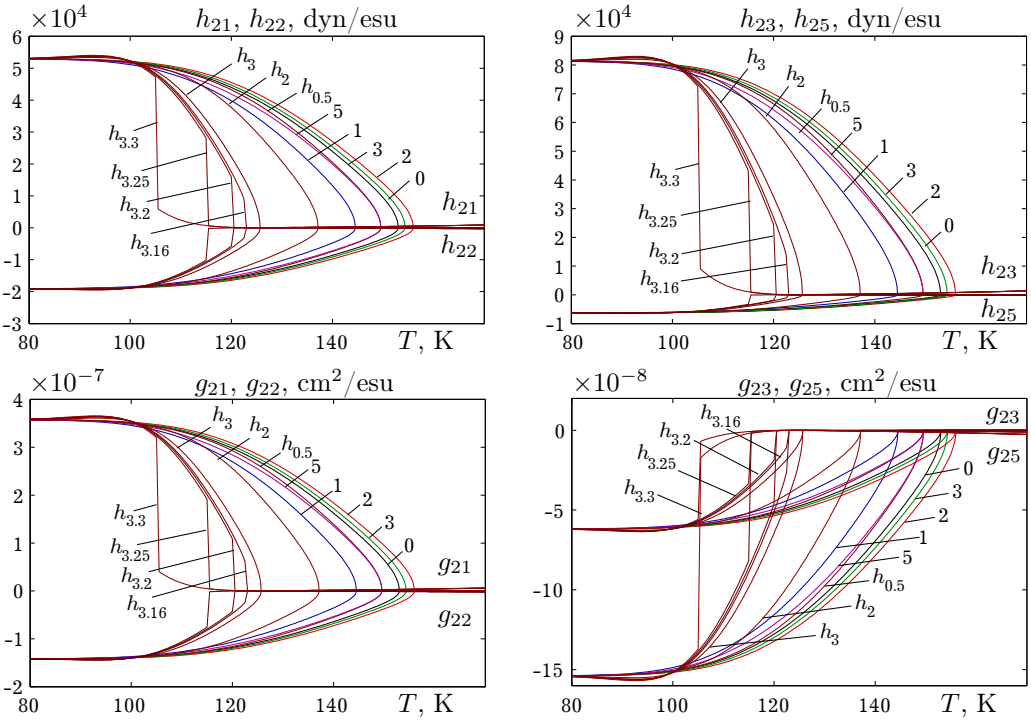

Fig. 10. The temperature dependences of the piezoelectric voltage h_{2l} and strain g_{2l} constants: at ambient pressure — 0, at pressures of different symmetries, each with the magnitude of 0.5 GPa: uniaxial p_1 — 1, p_2 — 2, p_3 — 3, shear stress σ_5 — 5, and under hydrostatic pressure (GPa): 0.5 — $h_{0.5}$, 2 — h_2, 3 — h_3, 3.12 — $h_{3.12}$, 3.15 — $h_{3.15}$.

The values of the piezomodules e_{21}, e_{23}, d_{21}, h_{21}, h_{23}, g_{21} and the absolute values of e_{22}, e_{25}, d_{22}, d_{23}, d_{25}, h_{22}, h_{25}, g_{22}, g_{23}, g_{25} decrease with increasing pressures p_2 and p_3 and increase with pressures p_1, p_h and stress σ_5 (Figs. 11, 12, 13).

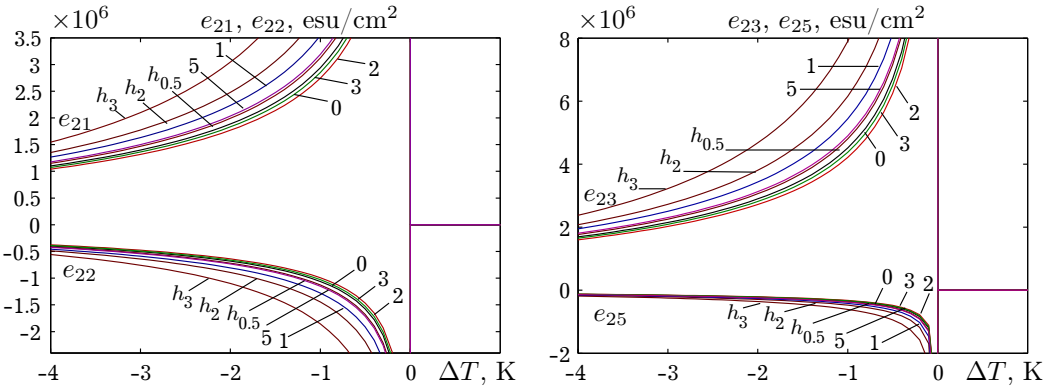

Fig. 11. Dependence of the piezoelectric voltage coefficients e_{2l} on the temperature difference $\Delta T = T - T_c$: at ambient pressure — 0, at pressures of different symmetries, each with the magnitude of 0.5 GPa: uniaxial p_1 — 1, p_2 — 2, p_3 — 3, shear stress σ_5 — 5, and under hydrostatic pressure (GPa): 0.5 — $h_{0.5}$, 2 — h_2, 3 — h_3.

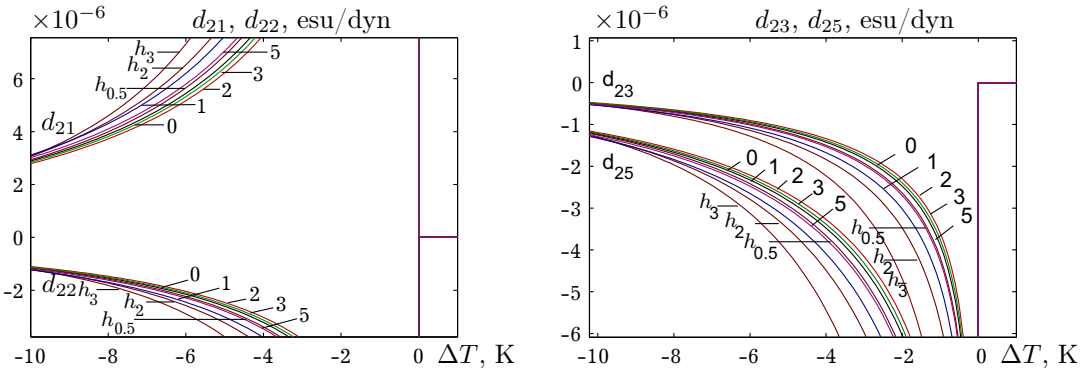

Fig. 12. Dependence of the piezoelectric strain coefficients d_{2l} on the temperature difference $\Delta T = T - T_c$: at ambient pressure — 0, at pressures of different symmetries, each with the magnitude of 0.5 GPa: uniaxial p_1 — 1, p_2 — 2, p_3 — 3, shear stress σ_5 — 5, and under hydrostatic pressure (GPa): 0.5 — $h_{0.5}$, 2 — h_2, 3 — h_3.

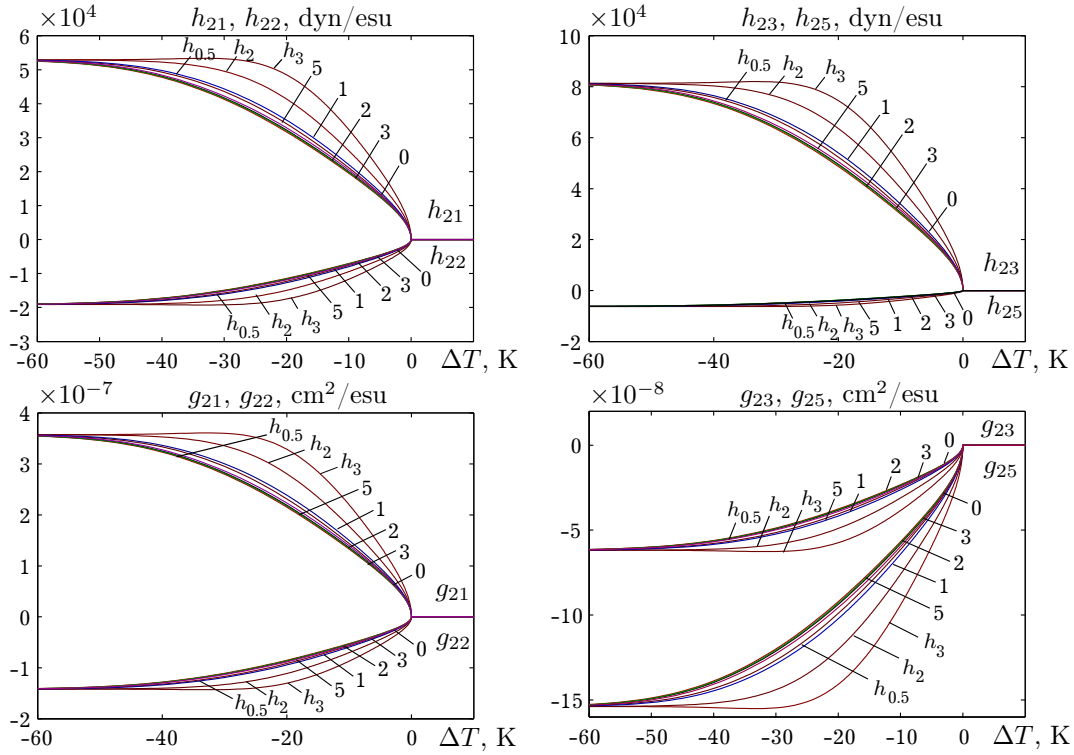

Fig. 13. Dependence of the piezoelectric voltage h_{2l} and strain g_{2l} constants on the temperature difference $\Delta T = T - T_c$: at ambient pressure — 0, at pressures of different symmetries, each with the magnitude of 0.5 GPa: uniaxial p_1 — 1, p_2 — 2, p_3 — 3, shear stress σ_5 — 5, and under hydrostatic pressure (GPa): 0.5 — $h_{0.5}$, 2 — h_2, 3 — h_3.

5. Conclusions

In the present work, within the framework of the modified proton ordering model for the quasi-one-dimensional hydrogen bonded ferroelectrics of the CsH_2PO_4 type, with taking into account the linear over the strains ε_i and ε_5 contributions into the energy of the proton system, and within the two-particle cluster approximation, we study the influence of hydrostatic and uniaxial pressures and shear stress σ_5 on the phase transition and physical properties of the CDP crystal. It is established that these stresses change the strains ε_i, ε_5, which leads to the stress dependences of the transition temperature and other characteristics of these crystals.

The behavior of spontaneous polarization, static dielectric permittivity, elastic constants, and piezoelectric coefficients at pressures up to 0.5 GPa, as well as the behavior of elastic constants and piezoelectric coefficients under hydrostatic pressure below and above the critical one is explored.

[1] Yasuda N., Okamoto M., Shimizu H., Fujimoto S., Yoshino K., Inuishi Y. Pressure-induced antiferroelectricity in ferroelectric CsH_2PO_4. Phys. Rev. Lett. **1**, 1311–1314 (1978).

[2] Yasuda N., Fujimoto S., Okamoto M., Shimizu H., Yoshino K., Inuishi Y. Pressure and temperature dependence of the dielectric properties of CsH_2PO_4 and CsH_2PO_4. Phys. Rev. B. **20**, 2755–2764 (1979).

[3] Schuele P. J., Thomas R. A. A structural study of the high-pressure antiferroelectric phase of CsH_2PO_4. Japanese Journal of Applied Physics. **24** (S2), 935, (1985).

[4] Marchon D., Novak A. Antiferroelectric Fluctuations in CsH_2PO_4 and Raman Spectroscopy. Ferroelectrics. **55** (1), 55–58 (1984).

[5] Brandt N. B., Zhukov S. G., Kulbachinskii V. A., Smirnov P. S., Strukov B. A. Influence of hydrostatic pressure on the dielectric properties of CsH_2PO_4. Phys. Solid State. **28**, 3159 (1986), (in Russian).

[6] Kobayashi Yu., Deguchi K., Azuma Sh., Suzuki E., Ming Li Ch., Endo Sh., Kikegawad T. Phase Transitions in CsH_2PO_4 Under High Pressure. Ferroelectrics. **285** (1), 83–89 (2003).

[7] Magome E., Tomiaka S., Tao Y., Komukae M. Pressure Effect on Phase Transition in Partially Deuterated $Cs(H_{1-x}D_x)_2PO_4$. J. Phys. Soc. Jpn. **79** (2), 025002 (2010).

[8] Gesi K., Ozawa K. Effect of hydrostatic pressure on the ferroelectric phase transitions in CsH_2PO_4 and CsH_2PO_4. Japanese Journal of Applied Physics. **17** (2), 435–436 (1978).

[9] Blinc R.,Baretto F. C. Sa. Ferroelectric and antiferroelectric dynamics of pseudo-one-dimensional CsH_2PO_4. J. Chem. Phys. **72** (11), 6031–6034 (1980).

[10] Stasyuk I. V., Levitskii R. R., Zachek I. R., Shchur Ya. J., Kutny I. V., Myts Ye. V. Influence of hydrostatic pressure on the phase transition, thermodynamic and dynamic properties of quasi-one-dimensional ferroelecric compounds with hydrogen bonds. Preprint ICMP, Ac. Sci UkrSSR, ICMP-91-4R (1991), (in Russian).

[11] Stasyuk I. V., Biletskii I. N. On the influence of hydrostatic and uniaxial stress on the ferroelectric phase transition in the KH_2PO_4 crystals. Bull. Ac. Sci. USSR, Phys. Ser. **4**, 705 (1983), (in Russian).

[12] Braeter H., Plakida N. M., Windseh W. On the pressure dependence of the phase transition temperature in hydrogen-bonded ferroelectrics. Solid State Communications. **69** (3), 289–292 (1989).

[13] Zachek I. R., Levitsky R. R., Vdovych A. S. Longitudinal static dielectric, piezoelectric, elastic, dynamic and thermal properties of quasi-one-dimensional CsH_2PO_4 type ferroelectrics with hydrogen bonds. Preprint ICMP-11-17U, Lviv (2011).

[14] Levitskii R. R., Zachek I. R., Vdovych A. S. Longitudinal Static Dielectric, Piezoelectric Elastic And Thermal Properties of Quasi-One-Dimensional CsH_2PO_4 Type Ferroelectrics. Phys. Chem. Solid St. **13** (1), 40–47 (2012).

[15] Deguchi K., Okaue E., Ushio S., Nakamura E., Abe K. Dilatometric Study of the Phase Transition of Quasi-One-Dimensional Ferroelectric CsH_2PO_4. J. Phys. Soc. Jpn. **53**, 3074–3080 (1984).

[16] Van Troeye B., van Setten M. J., Giantomassi M., Torrent M., Rignanese G.-Ma., Gonze X. First-principles study of paraelectric and ferroelectric CsH_2PO_4 including dispersion forces: Stability and related vibrational, dielectric, and elastic properties. Phys. Rev. B. **95** (2), 024112 (2017).

[17] Stasyuk I. V., Levitskii R. R., Korinevskii N. A. Collective vibrations of protons in compounds of KH_2PO_4-type. The cluster approximation. Phys. Stat. Sol. (b). **91** (2), 541–550 (1979).

[18] Praver S., Smith T. F., Finlaypon T. R. The Room Temperature Plastic Behaviour of CsH_2PO_4. Aust. J. Phys. **38** (1), 63–84 (1985).

Вплив одновісних та гідростатичного тисків, зсувної напруги σ_5 на фазові переходи та термодинамічні характеристики квазіодновимірних сегнетоелектриків типу CsH_2PO_4

Вдович А. С.[1], Зачек І. Р.[2], Левицький Р. Р.[1], Моїна А. Р.[1]

[1] *Інститут фізики конденсованих систем НАН України, вул. Свєнціцького, 1, Львів, 79011, Україна*
[2] *Національний університет "Львівська політехніка", вул. С. Бандери, 12, Львів, 79013, Україна*

У межах модифікованої моделі протонного впорядкування квазіодновимірних сегнетоелектриків з водневими зв'язками типу CsH_2PO_4 з врахуванням лінійних за деформаціями ε_i та ε_5 внесків в енергію протонної системи, але без врахування тунелювання в наближенні двочастинкового кластера, досліджено вплив одновісних p_i та гідростатичного p_h тисків, зсувної напруги σ_5 на фазовий перехід, поляризацію, поперечну діелектричну проникність, пружні сталі та п'єзомодулі сегнетоелектрика CsH_2PO_4. За належного вибору мікропараметрів отримано добрий кількісний опис відповідних експериментальних даних для цих кристалів.

Ключові слова: *сегнетоелектрики, діелектрична проникність, п'єзомодулі, зсувна напруга.*